Potential applicability of polyethyleneimine PEI-coated Eu_2O_3 and Dy_2O_3 nanoparticles for contrast enhancement in computed tomography

NANO EXPRESS

OPEN ACCESS

RECEIVED
6 December 2020

REVISED
30 January 2021

ACCEPTED FOR PUBLICATION
4 February 2021

PUBLISHED
15 February 2021

PAPER

Potential applicability of polyethyleneimine PEI-coated Eu_2O_3 and Dy_2O_3 nanoparticles for contrast enhancement in computed tomography

Valentina Olifirenko[1,7], Aiganym Abduraimova[1,7], Moon Sung Kang[2], Iruthayapandi Selestin Raja[2], Bakyt Duisenbayeva[3], Anara Molkenova[4,*], Laura Khamkhash[5], Yoon-Hwae Hwang[6], Dong-Wook Han[2,*] and Timur Sh Atabaev[4,*]

[1] Department of Biology, Nazarbayev University, Nur-Sultan 010000, Kazakhstan
[2] Department of Cogno-Mechatronics Engineering, College of Nanoscience and Nanotechnology, Pusan National University, Busan 46241, Republic of Korea
[3] Department of Radiology, Green Clinic, Nur-Sultan 010000, Kazakhstan
[4] Department of Chemistry, Nazarbayev University, Nur-Sultan 010000, Kazakhstan
[5] Core Facilities, Nazarbayev University, Nur-Sultan 010000, Kazakhstan
[6] Department of Nanoenergy Engineering and BK21 PLUS Nanoconvergence Technology Division, Pusan National University, Busan 46241, Republic of Korea
[7] These authors contributed equally.
[*] Authors to whom any correspondence should be addressed.

E-mail: anara.molkenova@nu.edu.kz, nanohan@pusan.ac.kr and timur.atabaev@nu.edu.kz

Keywords: Eu_2O_3, Dy_2O_3, nanoparticles, CT contrast agents, cytotoxicity, polyethyleneimine

Abstract

Rare-earth metal oxide nanoparticles considered promising contrast agents for x-ray computed tomography (CT) and magnetic resonance imaging (MRI). The main purpose of this study is to investigate the potential applicability of polyethyleneimine (PEI)-coated Eu_2O_3 and Dy_2O_3 nanoparticles (NPs) for CT x-ray attenuation. Morphology and other physicochemical properties of prepared samples were systematically investigated using a range of characterization tools. Preliminary cytotoxicity experiments with L-929 fibroblastic cells suggested that both samples have no significant toxicity at concentrations below 100 μg ml^{-1}. Clinical CT analysis shows that PEI@Eu_2O_3 NPs exhibit higher x-ray attenuation efficiency (~8 HU mM^{-1}) as compared to PEI@Dy_2O_3 NPs (~5 HU mM^{-1}).

1. Introduction

Lanthanide elements are widely used for the preparation of phosphorescent powders, glasses, permanent magnets, electronic components, etc Recently, nanostructures based on lanthanide elements attracted considerable interest in biomedical sciences because of the high density of heavy atoms per unit area and their excellent paramagnetic properties [1, 2]. For example, small Gd_2O_3 NPs are often used as potential contrast agents for magnetic resonance imaging (MRI), and computed tomography (CT) [3, 4]. Other nanostructures based on lanthanides such as Dy_2O_3, Yb_2O_3, Eu_2O_3, Ho_2O_3, and their mixtures were also efficient for CT, MRI, and optical imaging of cells [4–8]. In general, some lanthanide oxide-based NPs show higher water proton relaxivity rates as compared to their molecular counterparts [9]. Typically, each nanoparticle contains a large number of metal ions located on the surface, which in turn explains the contrast enhancement. In addition, lanthanide-based NPs can efficiently attenuate hard x-ray thanks to their high attenuation coefficients [10]. Recent studies suggested that some rare earth oxide-based NPs show better x-ray attenuation as compared to iodine-based complexes making them promising in CT scanning [4, 5, 10].

To date, nanocrystals of lanthanide oxides were fabricated in organic solvents such as glycols. From one side, the constant usage of toxic organic solvents can cause some occupational health risks. On the other hand, unreacted part of lanthanide salts together with glycols generate chemical wastes that require further utilization. Therefore, a green approach should be introduced for the fabrication of lanthanide-based contrast agents. From

this point of view, environment-friendly and low-cost urea homogeneous precipitation is an attractive method for the preparation of lanthanide oxides [8, 11]. In this method, urea dissolved in water is decomposed at elevated temperatures, which slowly increases the pH of the solution. As a result, a colloidal solution containing spherical-shaped lanthanide-based NPs can be obtained.

The toxicity of NPs is an important parameter that should be considered for potential applications in biomedicine. Numerous reports suggested that the toxicity of the NPs strongly depends on different parameters such as size, shape, and surface functional groups [12–14]. Various surface functional groups such as polyacrylic acid (PAA), polyethylene glycol (PEG), polyvinylpyrrolidone (PVP), and polyethyleneimine (PEI) are commonly used to improve the biocompatibility and colloidal stability of nanostructures [4, 8, 15–17]. Among them, a cationic polymer such as polyethyleneimine (PEI) can create positive charges on the surface resulting in steric and electrostatic stabilization of nanostructures. To the best of our knowledge, synthesis and PEI-functionalization of Eu_2O_3 and Dy_2O_3 NPs using green approaches were not reported so far. Therefore, the main objectives of this study are a) preparation of PEI-coated Eu_2O_3 and Dy_2O_3 NPs using green protocols, b) preliminary cytotoxicity assessment of PEI-coated Eu_2O_3 and Dy_2O_3 NPs, and c) testing the PEI-coated Eu_2O_3 and Dy_2O_3 NPs as x-ray CT contrast agents.

2. Methods

2.1. Synthesis of nanoparticles

High purity materials were purchased from Merck and used as received. For the fabrication of Eu_2O_3 and Dy_2O_3 nanoparticles, 0.5 mM of $EuCl_3 \times 6H_2O$ (99.9%) or $DyCl_3 \times 6H_2O$ (99.9%) were dissolved in 50 ml of ultrapure water. Next, 0.5 g of urea (99.0%–100.5%) was added to the prepared solution. The final solutions were heated at 90 °C for 2 h in closed Duran glass bottles (100 ml capacity). Formed precipitates were collected by centrifugation process, dried, and calcined in air at 700 °C for 1 h. The coating of the NPs with PEI was performed according to a reported protocol [17] with a slight modification. In brief, 60 mg of NPs were ultrasonically dispersed in 5 ml of ultrapure water for several minutes. Next, the solution pH was adjusted to 10 with the help of 0.1 M NaOH. Finally, 0.5 ml of PEI was added and the resulting solution was left for 24 h under constant stirring. PEI-coated NPs were collected, gently rinsed with ultrapure water two times, and naturally dried.

2.2. Characterization

Transmission electron microscope TEM JEM 3010 (JEOL Ltd) was used for morphology and size analysis of prepared NPs. The size and zeta potential of prepared NPs were analyzed using Nanotrac Wave II Q (Microtrac MRB). Structural analysis of prepared samples was performed using a Rigaku SmartLab (Rigaku Corporation) x-ray diffraction system. Fourier transform infrared absorption spectrophotometer FTIR Nicolet iS5 (Thermo Fisher Scientific) was used to analyze the surface coating of NPs. Thermal Gravimetric Analysis (TGA) measurements were performed using Simultaneous Thermal analyzer STA-6000 (PerkinElmer Inc.). PEI-coated NPs were heated from ambient temperature up to 600 °C at a rate of 10 °C per minute. Nitrogen was used as a purge gas (flow rate 20 ml/min). Commercial Phillips Brilliance 64 CT scanner (Phillips) was used for x-ray attenuation experiments. The following conditions were used during measurements: the x-ray source voltage 120 kV, current = 482 mA, the field of view FOV = 350 mm, and slice thickness = 1 mm. All measurements were performed at room temperature.

2.3. Cell culture

L-929 cells (a murine fibroblast cell line from subcutaneous connective tissue) were cultured in Dulbecco's modified Eagle's medium supplemented with 10% fetal bovine serum and 1% antibiotic-antimycotic solution (including 10,000 units penicillin, 10 mg streptomycin, and 25 mg amphotericin B per ml) at 37 °C in a humidified atmosphere of 5% CO_2 in the air. The cells (1×10^5 cells/well) were seeded into well plates and incubated for growth to confluence overnight.

2.4. Cytotoxicity assay

The cell viability was examined by a cell counting kit − 8 (CCK-8, Dojindo Lab.) assay, containing highly water-soluble tetrazolium salt [WST-8, 2-(2-methoxy-4-nitrophenyl)- 3-(4-nitrophenyl)-5-(2,4-disulfophenyl)-2H-tetrazolium, monosodium salt], which is reduced to a yellow color formazan dye by mitochondrial dehydrogenases. After treated with different concentrations of NPs, the cells were incubated with WST-8 for the last 4 h of the culture periods (24 h) at 37 °C in the dark. The absorbance was measured at 450 nm using a SpectraMax 340 ELISA reader (Molecular Device Co.). Cell viability was calculated by the percentage ratio of the optical density of the supernatants of each well.

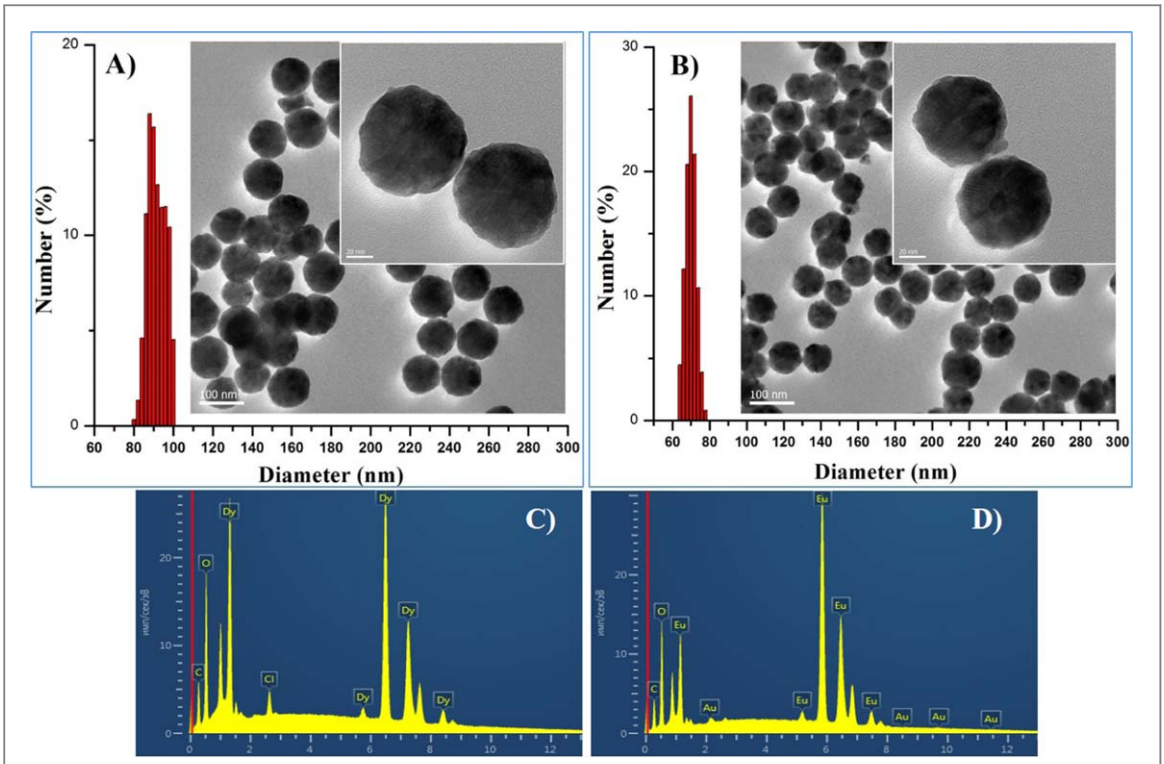

Figure 1. Size distribution and TEM microphotographs of (A) PEI@Dy_2O_3 NPs, and (B) PEI@Eu_2O_3 NPs, scale bar—100 nm (Inset are high magnification TEM images of NPs, scale bar—20 nm). EDX analysis of (C) PEI@Dy_2O_3 NPs, and (d) PEI@Eu_2O_3 NPs.

2.5. Statistical analysis

All variables were tested in three independent cultures for cytotoxicity assay, which was repeated twice ($n = 6$). Statistical analysis was performed using one-way ANOVA, followed by a Bonferroni test for multiple comparisons. Quantitative data are expressed as the mean $\pm$ standard deviation (SD). The value of $P < 0.05$ was considered statistically significant.

3. Results and Discussion

TEM analysis was utilized to evaluate the morphology of the prepared PEI-coated NPs. The inset of figures 1(A) and (B) shows that NPs with nearly spherical morphology were obtained in both cases. Detailed inspection of NPs revealed that both samples have different sizes despite identical synthesis conditions. In particular, the measured size of PEI@Dy_2O_3 NPs was in the range of 79–102 nm, while the size of PEI@Eu_2O_3 NPs was in the range of 67–79 nm. It should be noted that no agglomeration of PEI-coated NPs was observed during the TEM analysis. Figures 1(C) and (D) shows the chemical analysis of prepared samples performed by Energy Dispersive x-ray EDX analysis. One can see that Eu, Dy, O, and C elements are easily detectable suggesting the formation of PEI-coated metal oxide NPs.

Zeta potential measurements of PEI@Dy_2O_3 NPs (+14.3 mV) and PEI@Eu_2O_3 NPs (+16.9 mV) suggested that positive charges formed on the surface of NPs due to PEI coating. Figure 2 shows digital images of as-prepared NPs dispersed in simulated body fluid (SBF) solution. One can see that these NPs can be easily dispersed in SBF, but colloidal dispersions can be stable for a limited time only. In particular, first precipitates can be found after 6 h of storage, while the majority of NPs can be found at the bottom within the first 18 h. This can be explained by the fact that these NPs have moderate zeta potential values. Therefore, additional in-vivo experiments are required to confirm the bio-stability of prepared NPs. Nevertheless, a colloidal solution of NPs can be easily formed again by sonication or even slight shaking.

Figure 3(A) shows the XRD patterns of PEI@Dy_2O_3 and PEI@Eu_2O_3 NPs. One can easily assign the observed strong peaks to pure cubic phases of corresponding lanthanide oxides (JCPDS # 86-2476 for Eu_2O_3 and JCPDS# 10-0059 for Dy_2O_3) [18]. The broad peaks at lower angles due to amorphous PEI-coating were not detected. Next, FTIR analysis (figure 3(B)) was utilized to confirm the presence of the organic PEI coating on the surface of Dy_2O_3 and Eu_2O_3 NPs. Absorption peaks observed at 561 cm^{-1} and 519 cm^{-1} were assigned to the bending vibrations of Dy-O and Eu-O bands, respectively [19, 20]. The peak observed at 850 cm^{-1} was assigned to the bending vibration of the C–H bond [21]. The split peak around 1512 and 1402 cm^{-1} was attributed to

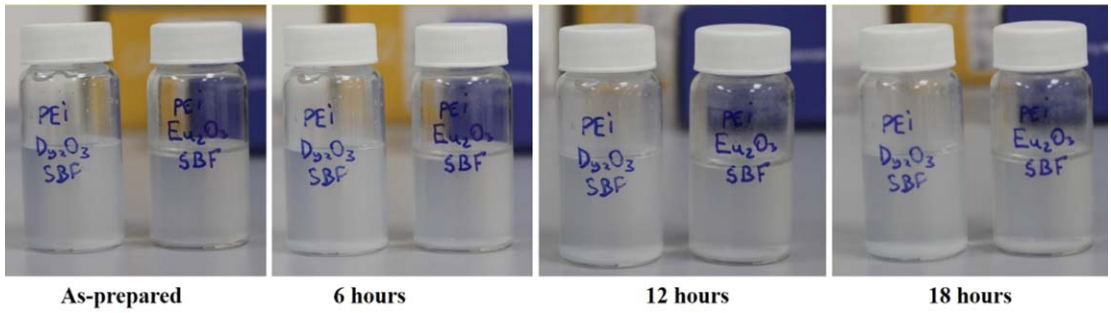

Figure 2. Digital images showing the colloidal stability of prepared NPs in SBF.

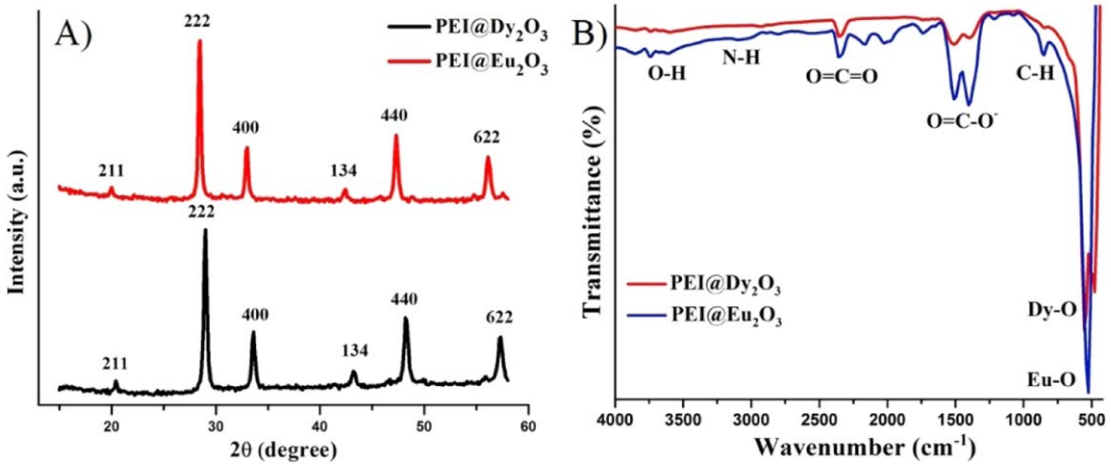

Figure 3. (A) XRD patterns and (B) FTIR analysis of PEI-coated NPs.

symmetric and asymmetric stretching vibrations of the carboxyl group [19]. The trapped carbon dioxide displayed absorption around 2350 m^{-1} [21]. The broad absorption band from 3100 to 3500 cm^{-1} corresponds to the aliphatic primary amine N–H bond stretching vibrations [21]. The absorption in the region from 3500 and 3700 cm^{-1} was caused by O–H bond bending vibrations from the absorbed moisture [21]. One can observe that the absorption peaks for Eu_2O_3 NPs were stronger compared to Dy_2O_3 NPs. This could be attributed to the size difference of prepared samples. Smaller sized Eu_2O_3 NPs have a bigger active surface area that can potentially accommodate a larger number of functional groups as compared to Dy_2O_3 NPs.

Next, TGA analysis was performed to estimate the amount of PEI coating in prepared samples. Figure 4 shows the TGA curves for PEI-coated NPs measured in the range of 20°C–600°C. The PEI-coated NPs exhibited the first weight loss of about 2.8% and 2.9%, for PEI@Dy_2O_3 and PEI@Eu_2O_3 respectively, at the range of 20 °C–225 °C, which could be attributed to the evaporation of physisorbed and chemisorbed water [22]. The second weight loss above 225 °C equal to approximately 13.8% and 13.1% for PEI@Eu_2O_3 and PEI@Dy_2O_3 NPs, respectively, correspond to the PEI coating amount in the samples. By considering these weight losses, the total amounts of Eu_2O_3 and Dy_2O_3 in the samples are 83.3% and 84.1%, respectively.

Preliminary cytotoxicity analysis of PEI-coated NPs has been performed to access the safety of prepared samples. L-929 mouse fibroblast cells were cultured with different NPs concentrations up to 200 $\mu g\ ml^{-1}$. Figure 5 displays the cytotoxicity profiles of PEI-coated NPs which clearly revealed a dose-dependent trend. In both samples, a significant decrease in cell viability was found after the threshold of 100 $\mu g\ ml^{-1}$. In literature, 80% of cell viability is usually accepted as a relative indicator of non-toxicity [23]. By considering this assumption, one can assume that these PEI-coated NPs show no significant toxicity at concentrations below 100 $\mu g\ ml^{-1}$. On the other hand, lanthanide-based NPs can be toxic to other cell lines. Therefore, it is very important to mention that the toxicity of prepared PEI-coated NPs must be studied with other cell lines, by other end-point viability measurements, and *in-vivo*.

A commercial CT scanner was further utilized to demonstrate the potential applicability of PEI@ Dy_2O_3 and PEI@Eu_2O_3 NPs for x-ray attenuation. Figure 6 shows the x-ray phantom images of PEI@Eu_2O_3 NPs (A) and PEI@Dy_2O_3 NPs (B) water suspensions at two concentrations. Two different concentrations, i.e. 0.5 mM and 1

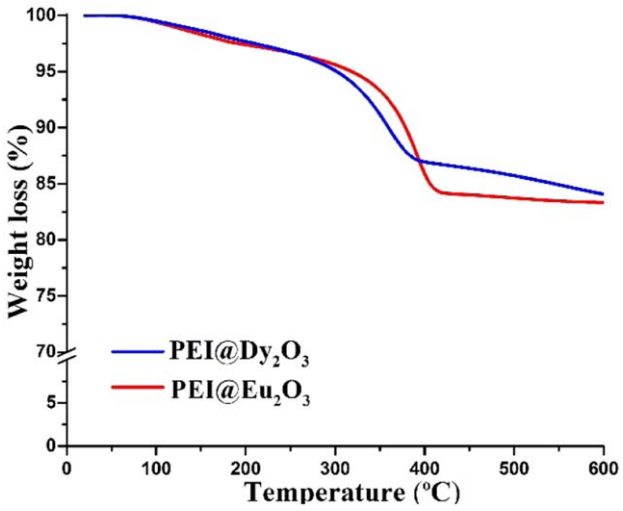

Figure 4. TGA curves of PEI-coated NPs.

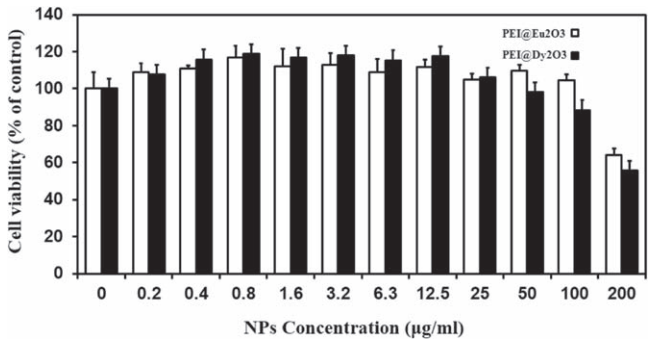

Figure 5. Dose-dependent cytotoxicity profiles of PEI-coated NPs.

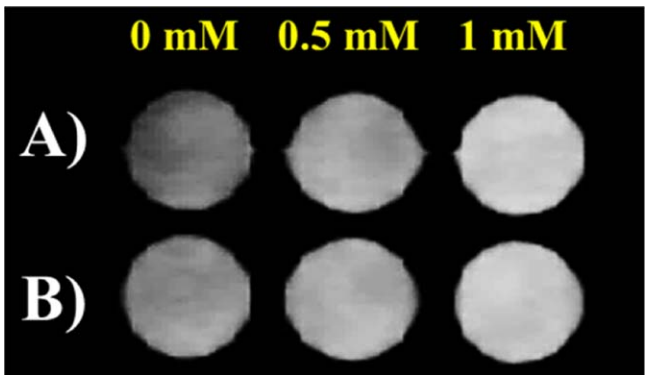

Figure 6. X-ray phantom images of (A) PEI@Eu_2O_3, and (B) PEI@Dy_2O_3 NPs.

mM were tested to observe the contrast enhancement trend with increasing of NPs concentration. Phantom images of pure water (0 mM) were also supplied for comparison. One can observe that the contrast of the phantom images obviously enhanced (become brighter) in suspensions with NPs compared to pure water. In literature, the x-ray attenuation efficiencies (η), i.e. Hounsfield Units HU per 1 mM of metal atomic concentration typically measured for comparison. The HU values per 1 mM of metal concentration for PEI@Eu_2O_3 and PEI@Dy_2O_3 were found to be $\sim$8 and $\sim$5 HU mM^{-1}, respectively. The literature data has shown that the observed x-ray attenuation efficiencies (HU/mM) of the examined NPs are relatively higher than that of commercial iodine contrast agent (Ultravist®, 4.4 HU mM^{-1}) [4]. One can also notice that the x-ray

attenuation efficiency of PEI@Eu_2O_3 NPs was significantly higher compared to PEI@Dy_2O_3 NPs. Thus, PEI@Eu_2O_3 NPs bearing better potential to be applied as a promising x-ray CT contrast agent.

4. Conclusions

In conclusion, PEI-coated Dy_2O_3 and Eu_2O_3 NPs were prepared and investigated their applicability as potential CT contrast agents. The proposed green and low-cost fabrication method allows fast synthesis of the spherical-shaped NPs at large scales. Preliminary cytotoxicity analysis with L-929 cells revealed that prepared samples have no significant toxicity at concentrations below 100 μg ml^{-1}. X-ray attenuation experiments suggested that PEI@Eu_2O_3 NPs have better x-ray attenuation efficiency of ~8 HU mM^{-1} compared to PEI@Dy_2O_3 NPs with a value of ~5 HU mM^{-1}. Therefore, PEI@Eu_2O_3 NPs can be considered as a promising candidate for x-ray attenuation purposes.

Acknowledgments

This study was funded by the National Research Foundation of Korea (NRF) grant funded by the Korea government (MSIT) (No. 2019R1A4A1024116). This work was supported by the National Research Foundation of Korea (NRF) grant funded by the Korea government (MSIT) (No. 2020R1A2C2007590) Aiganym Abduraimova would like to thank the FRIP grant provided by Young Researchers Alliance.

Data availability statement

All data that support the findings of this study are included within the article (and any supplementary files).

Conflict of interests

The authors have no conflicts of interest.

ORCID iDs

Anara Molkenova https://orcid.org/0000-0003-0351-7622
Yoon-Hwae Hwang https://orcid.org/0000-0002-1982-2210
Dong-Wook Han https://orcid.org/0000-0001-8314-1981
Timur Sh Atabaev https://orcid.org/0000-0001-7252-4098

References

[1] Dong H, Du S R, Zheng X Y, Lyu G M, Sun L D, Li L D, Zhang P Z, Zhang C and Yan C H 2015 Lanthanide nanoparticles: from design toward bioimaging and therapy *Chem. Rev.* **115** 10725–815
[2] Kwon H J, Shin K, Soh M, Chang H, Kim J, Lee J, Ko G, Kim B H, Kim D and Hyeon T 2018 Large scale synthesis and medical applications of uniform-sized metal oxide nanoparticles *Adv. Mater.* **30** 1704290
[3] Park J Y, Kim S J, Lee G H, Jin S, Chang Y, Bae J E and Chae K S 2015 Varyous ligand-coated ultrasmall gadolinium-oxide nanoparticles: water proton relaxivity and in-vitro T_1 MR image *J. Korean Phys. Soc.* **66** 1295–302
[4] Ghazanfari A *et al* 2019 Synthesis, characterization, and x-ray attenuation properties of polyacrylic acid-coated ultrasmall heavy metal oxide (Bi_2O_3, Yb_2O_3, $NaTaO_3$, Dy_2O_3, and Gd_2O_3) nanoparticles as potential CT contrast agents *Colloid. Surface. A.* **576** 73–81
[5] Liu Z, Li Z, Liu J, Gu S, Yuan Q, Ren J and Qu X 2012 Long-circulating Er^{3+} -doped Yb_2O_3 up-conversion nanoparticle as an *in vivo* x-ray CT imaging contrast agent *Biomaterials* **33** 6748–57
[6] Chaudharry S and Umar A 2016 Glycols functionalized fluorescent Eu_2O_3 nanoparticles: Functionalization effect on the structural and optical properties *J. Alloys Compd.* **682** 160–9
[7] Xu W, Bony B A, Kim C R, Baeck J S, Chang Y, Bae J E, Chae K S, Kim T J and Lee G H 2013 Mixed lanthanide oxide nanoparticles as dual imaging agent in biomedicine *Sci. Rep.* **3** 3210
[8] Atabaev T S, Shin Y C, Song S J, Han D W and Hong N H 2017 Toxicity and T_2-weighted magnetic resonance imaging potentials of holmium oxide nanoparticles *Nanomaterials* **7** 216
[9] Dong H *et al* 2015 Lanthanide nanoparticles: From design toward bioimaging and therapy *Chem. Rev.* **115** 10725–815
[10] Lee G H, Chang Y and Kim T J 2014 *Ultrasmall Lanthanide Oxide Nanoparticles for Biomedical Imaging and Therapy* (Bungay: Woodhead Publishing Limited)
[11] Fukushima S *et al* 2016 Synthesis of Y_2O_3 nanophosphors by homogeneous precipitation method using excessive urea for cathodoluminescence and upconversion luminescence bioimaging *Opt. Mater. Express* **6** 831–43
[12] Barbalinardo M, Caicci F, Cavalinni M and Gentili D 2018 Protein corona mediated uptake and cytotoxicity of silver nanoparticles in mouse embryonic fibroblast *Small* **14** 1801219

[13] Kim T H, Kim M, Park H S, Shin U S, Gong M S and Kim H W 2012 Size-dependent cellular toxicity of silver nanoparticles *J. Biomed. Mater. Res. A* **100** 1033–43
[14] Raja I S *et al* 2019 Toxicity of zero- and one-dimensional carbon nanomaterials *Nanomaterials* **9** 1214
[15] Kim S H *et al* 2012 Synthesis of PEG-iodine-capped gold nanoparticles and their contrast enhancement in in-vitro and in-vivo for x-ray/CT *J. Nanomater.* **2012** 504026
[16] Lee H Y *et al* 2008 Synthesis and characterization of PVP-coated large core iron oxide nanoparticles as an MRI contrast agent *Nanotechnology* **19** 165101
[17] Lu W *et al* 2014 Facile synthesis and characterization of polyethyleneimine-coated Fe_3O_4 superparamagnetic nanoparticles for cancer cell separation *Mol. Med. Rep.* **9** 1080–4
[18] Zhu Y, Zhai X and Wang L 2013 Hydrothermal synthesis of $Ln(OH)_2$ nanorods and the conversion to Ln_2O_3 (Ln=Eu, Nd, Dy) nanorods via annealing process *J. Nanomater.* **2013** 130514
[19] Chandrasekhar M *et al* 2014 Comparison of structural and luminescence properties of Dy_2O_3 nanopowders synthesized by co-precipitation and green combustion routes *Mater. Res. Bull.* **55** 237–45
[20] Kang J G, Jung Y, Min B K and Sohn Y 2014 Full characterization of $Eu(OH)_3$ and Eu_2O_3 nanorods *Appl. Surf. Sci.* **314** 158–65
[21] Coates J 2000 Interpretation of infrared spectra, a practical approach ed R A Meyers *Encyclopedia of Analytical Chemistry* (Chichester: Wiley) 10815–37
[22] Saadatkhah N *et al* 2020 Experimental methods in chemical engineering: Thermogravimetric analysis—TGA *Can. J. Chem. Eng.* **98** 34–43
[23] Molkenova A *et al* 2019 Gd_2O_3 nanoparticles coated with a fluorescent carbon layer for potential T_1-weighted magnetic resonance and cells imaging *Nanosci. Nanotechnol. Lett.* **11** 813–7